



**HAL**  
open science

## Measurement of the temperature of burning aluminum particles using multi-spectral pyrometry

Valentin Glasziou, Christian Chauveau, Sébastien Courtiaud, Fabien Halter

► **To cite this version:**

Valentin Glasziou, Christian Chauveau, Sébastien Courtiaud, Fabien Halter. Measurement of the temperature of burning aluminum particles using multi-spectral pyrometry. *Combustion Science and Technology*, 2024, 196 (13), pp.2138-2151. 10.1080/00102202.2024.2378459 . hal-04652868

**HAL Id: hal-04652868**

**<https://cnrs.hal.science/hal-04652868v1>**

Submitted on 7 Aug 2024

**HAL** is a multi-disciplinary open access archive for the deposit and dissemination of scientific research documents, whether they are published or not. The documents may come from teaching and research institutions in France or abroad, or from public or private research centers.

L'archive ouverte pluridisciplinaire **HAL**, est destinée au dépôt et à la diffusion de documents scientifiques de niveau recherche, publiés ou non, émanant des établissements d'enseignement et de recherche français ou étrangers, des laboratoires publics ou privés.

## Measurement of the temperature of burning aluminum particles using multi-spectral pyrometry

*Valentin Glasziou<sup>1,2,\*</sup>, Christian Chauveau<sup>1</sup>, Sébastien Courtiaud<sup>2</sup>, Fabien Halter<sup>1</sup>*

<sup>1</sup>*ICARE CNRS, Orléans France*

<sup>2</sup>*CEA, DAM, CEA–Gramat, Gramat France*

*\*Corresponding author: valentin.glasziou@cnsr-orleans.fr*

### Abstract

Aluminum is used in the composition of many high explosives and contributes to their blast effect. This work focuses on the study of the combustion of a single isolated particle of size between 30 and 100  $\mu\text{m}$  in an arbitrary atmosphere, whose pressure and composition are chosen to be close to those encountered in a high-explosive fireball. This gaseous atmosphere is still largely unreferenced, and this work aims to provide a better understanding of combustion in this environment. The use of an electrostatic levitator coupled with multi-spectral pyrometric diagnostics enables us to select a single particle and measure its temperature during combustion. Photomultipliers (PMs) are used to follow the temporal evolution of the particle's light emission during combustion. In this work, we also used PMs as pyrometric devices to measure temperature. The diagnostic allows us to determine the temporal evolution of the integrated temperature of the condensed phase during combustion of the aluminum particle. By way of example, a temperature of 3300K was obtained for the combustion of Al in air at 1 bar. The data collected will also be used to verify the assumptions made in the combustion models (e.g. temperature stability during combustion).

### Keywords

Combustion; Aluminum; Temperature; Pyrometer

### Introduction

The analysis of the combustion of aluminum particles is of importance in many fields. A better understanding of the phenomenon and the constitution of databases on this potential energy source will allow a more efficient use of aluminum. An example of its current use is in rocket boosters with solid propellants, where it has been studied for several decades. Alternatively, it is also largely used in high explosives.

(Oran, 2015) defines an explosion as a phenomenon in which energy is released into space faster than it can dissipate itself, resulting in the formation of a shock wave. A common example of an explosion is that of a solid high explosive. The phenomenon is extremely exothermic and is defined as a reactive shock wave propagating through the high explosive and decaying into detonation products. These products in turn burn on contact with air; this is the afterburning stage. This last stage contributes significantly to the total energy released by the explosion. The use of metal particles in the explosive composition can enhance the effect of afterburning. Aluminum has an important role in this phase, when it is used in high explosives as demonstrated by (Fedina, 2017) and (Frost and Zhang, 2006). Aluminum

particles are heated by the detonation wave, then dispersed with the expansion of the gases and burn in a mixture composed of the detonation products and air. Additional heat is then produced within the fireball, making it more energetic as described by (Cooper et al., 2006). This zone is composed of air and detonation products ( $\text{CO}_2$ ,  $\text{CO}$ ,  $\text{H}_2\text{O}$ ). This phenomenon is also illustrated by the tests conducted at CEA-Gramat in Figure 1. Unfortunately, aluminum particles are difficult to follow and study during afterburning because of the rapidity and intensity of the phenomena (Suarez, 2020).

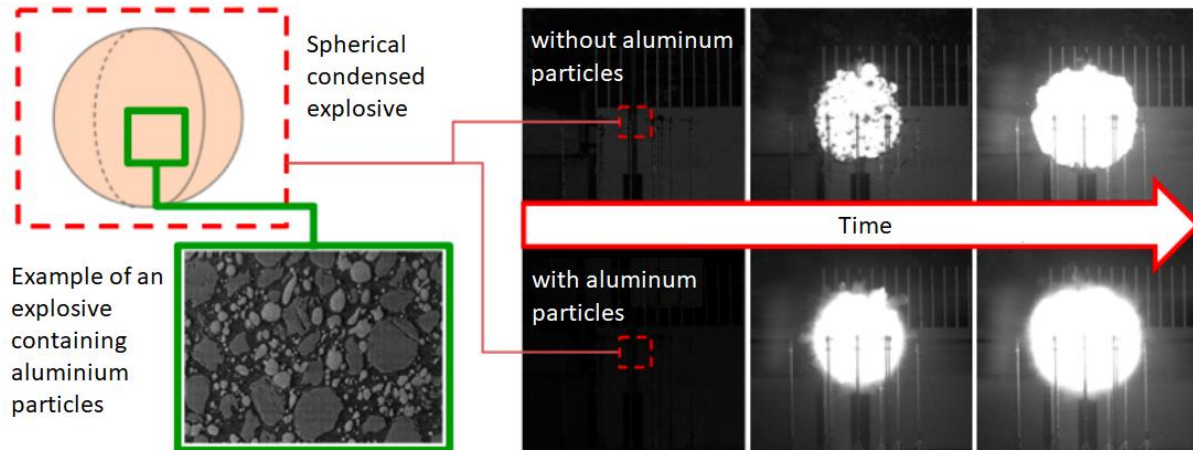


Figure 1 - Comparison of the afterburning of aluminized and non-aluminized explosives. Images were obtained from tests of spherical charges with aluminum particles on the bottom (B2213A) and without aluminum particles on the top (B2238A) (Suarez, 2020). Tests were performed at CEA-Gramat.

The study of the different reactions, depending on the environment of the particles, is therefore a major challenge for the understanding of aluminized explosives. In this context, the knowledge of information such as the combustion time and the temperature of the condensed phases is essential. To study this combustion during afterburning, a device that creates the environment encountered by a particle in the fireball will be used. It consists of the electrodynamic levitator. It allows you to isolate a single particle to study its combustion under the desired conditions. The aim of this paper is to describe the method used in this setup to measure the temperature of burning particles using a multi-spectral pyrometry method. This technique has been used in several aluminum studies (Chang et al., 2021, Dreizin, 1999, Millogo et al., 2020).

## 1. Experimental setup

The experimental setup used in this study has already been used in the thesis work of (Legrand, 2000, Marion, 1996) and (Braconnier, 2020). This chapter introduces the operation of the experimental setup used to study the fundamental combustion of micrometric aluminum particles.

### 1.1. Electrodynamic levitator

The fundamental study of the combustion of an individual aluminum particle is limited either by the group effects of Bunsen burners, or by the additional heat exchanges associated with the use of physical supports or aerodynamic levitation techniques. The electrodynamic levitator enables us to isolate a

single particle without any material support in a stable and repeatable position. It has already been used in various applications (Bar-Ziv and Sarofim, 1991, Davis et al., 1990, Hartung and Avedisian, 1992).

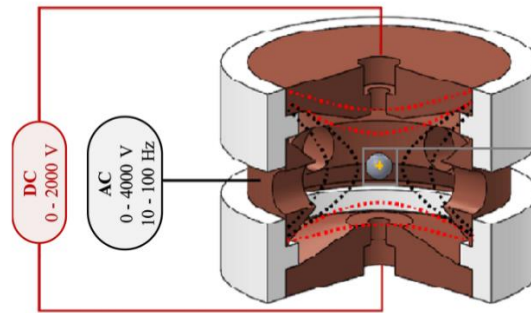


Figure 2 - Diagram of the electrodynamic levitator. (Braconnier, 2021)

The levitator works by superimposing DC and AC electric fields applied to a particle previously charged by friction which counteracts the force of gravity and guide it to the desired location. Electric fields are used to center the particle for reproducible experiments. Figure 2 shows a schematic representation of the levitator structure used during this study. The levitator, injection chamber and laser are the same as those used in the studies by (Legrand, 2000, Marion, 1996) and (Braconnier, 2020) and are described in more detail in their work (Braconnier, 2020) used a recent high-speed camera on the experimental set-up. In this study, we developed and implemented the entire pyrometry system.

## 1.2. High-pressure chamber

A high-pressure (HP) chamber is needed to study the combustion of the aluminum particle under parameterized conditions. The levitator is arranged inside the chamber as shown in the Figure 3. It is made up of metal parts in AU4G aluminum alloy. The center of the chamber is a cylinder closed at each end by a cover. The cylindrical shape has been chosen to withstand high pressures. The maximum pressure supported by the chamber is over 60 bar at ambient temperature. Gases are supplied by several gas lines equipped with pressure gauges. Pressurized cylinders, with high purity (more than 99.7%), containing the various required elements for the desired gaseous environment ( $O_2$ ,  $N_2$ ,  $CO$ , etc.) are located in an external room. Two digital pressure gauges (Keller), 10 & 100 bar with 0.1% full-scale accuracy, provide the absolute pressure in the chamber, enabling the composition of the medium to be accurately determined by the partial pressure of each species. To limit inaccuracy due to the different dead volumes induced by the vacuum operation, the chamber is filled with the desired gas mixture at high pressure (over 10 bar) before being evacuated again. This operation is repeated several times, to ensure that the mixture in the chamber is of the desired composition.

This HP chamber has several elements for injecting, igniting and visualizing particles. For injection a compensated piston is placed on the upper cover. Portholes are arranged in pairs opposite each other, halfway up the central cylinder. Two barium fluoride windows ( $BaF_2/ZKN7$ ) allows the entire visible spectrum to pass through.

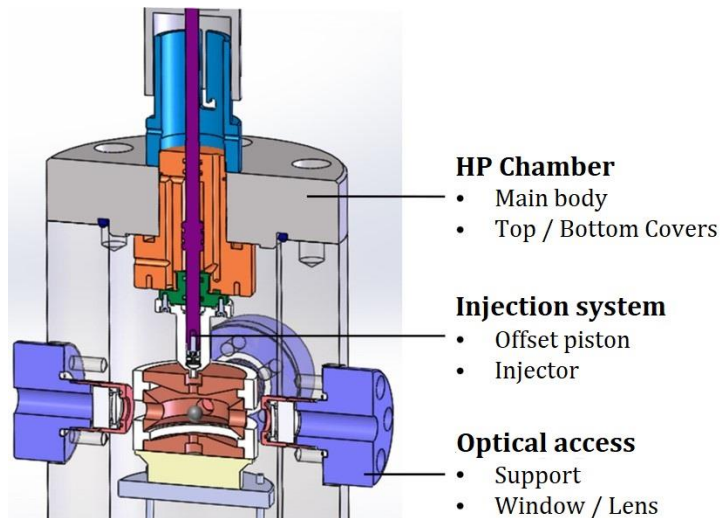


Figure 3 - Diagram of the instrumented high-pressure chamber containing the electrodynamic levitator (Braconnier, 2021)

For igniting the particle, two other accesses are provided to propagate and focus the laser beam. A focusing lens, with a focal length of 50.8 mm, is used to focus the laser at the center of the levitator. The lenses are made of zinc selenide (ZnSe), designed to efficiently transmit the radiation from the CO<sub>2</sub> laser.

### 1.3. Ignition system: CO<sub>2</sub> laser

A SYNRAD 48–5 CO<sub>2</sub> laser ( $\lambda_{\text{laser}} = 10.6 \mu\text{m}$ ) is used to provide the energy needed to ignite the particle. This laser was set up and studied by (Legrand, 2000). The only interaction noted was a rise of the particle temperature, without photodissociation effect. Once combustion has started, laser emission is interrupted by a trigger generated by the PM signal above a selected light intensity threshold. The stabilized levitated particle is heated almost uniformly on both sides by the initially bisected laser beam, as shown in Figure 4.

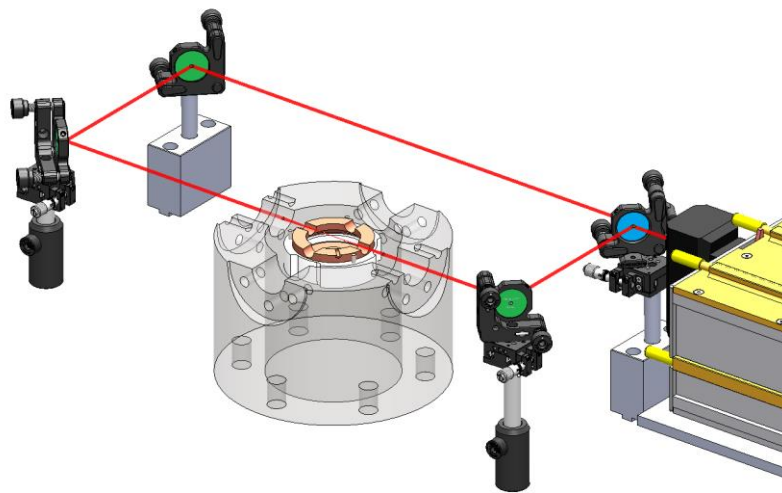


Figure 4 - Diagram of the SYNRAD 48-5 CO<sub>2</sub> laser path, 50/50 beam splitter in blue and gold-plated mirrors in green

The laser beam diameter is over 200  $\mu\text{m}$ , for a particle diameter of between 20 and 100  $\mu\text{m}$ . This allows uniform heating to be assumed.

The laser power can be set using an intermediate control. Its maximum operating power is 50 W, and the overall transmission coefficient of the optical path was measured at 0.85. The maximum laser intensity was used in the experiments described here as the power deposited only affects the ignition delay, without impacting the subsequent combustion sequence.

#### **1.4. Fast camera**

The temporal tracking of the evolution of the burning particle is ensured by the use of an imaging device coupling a fast PHANTOM camera combined with a long-distance microscope QUESTAR QM100 focused on the particle in reaction. The camera used is the PHANTOM TMX 7510, allowing 76 000 fps at maximum resolution ( $1280 \times 800 \text{ px}^2$ ) to 250 000 fps at the resolution used in this study ( $768 \times 768 \text{ px}^2$ ). The magnification obtained with the long-distance microscope is  $1.27 \mu\text{m}/\text{px}$ . The images obtained by the fast camera allow not only a phenomenological description of the combustion process, but also, after the application of a numerical post-processing, the extraction of quantitative information such as for example the diameter of the initial aluminum particle after melting, the temporal evolution of this diameter, the migration speed of the alumina particles toward the aluminum drop, etc.

## **2. Pyrometer and method for temperature measurement**

Bi-spectral optical pyrometry is the preferred method in our study, as it is non-intrusive. It makes it possible to determine the temporal evolution of the condensed phase temperature during combustion (Levendis et al., 1992, Monier et al., 2017, Panagiotou et al., 1996), and achieves greater accuracy than monochromatic pyrometry. For temperature measurements using optical pyrometry, the challenge is to transform the luminance measured into the actual temperature of the sample. Various types of optical pyrometer exist: their accuracy of measurement is directly related to the emissivity factor.

The photomultipliers (Thorlabs PMT1002) track the temporal evolution of the particle's overall light emission during combustion. They collect information on the radiative emission emitted by the particle as it burns, and transform it into voltage signals, enabling the luminous evolution of the combustion process to be monitored. This useful tool can also be used to control the extinction of the  $\text{CO}_2$  laser. These PMs are assembled on a same frame to form a pyrometer. This module makes it easy to exchange mirrors/emission dichroic filter sets and color filters. This configuration enables the detection of signals at three different wavelengths. The input port of the filter block has an SM1 thread ( $1.035''-40$ ). The module is equipped with an SMA fiber-optic connector for attaching a multimode optical fiber. The other end of this fiber is then connected to the optical system, consisting of lenses that focus on the center of the combustion chamber.

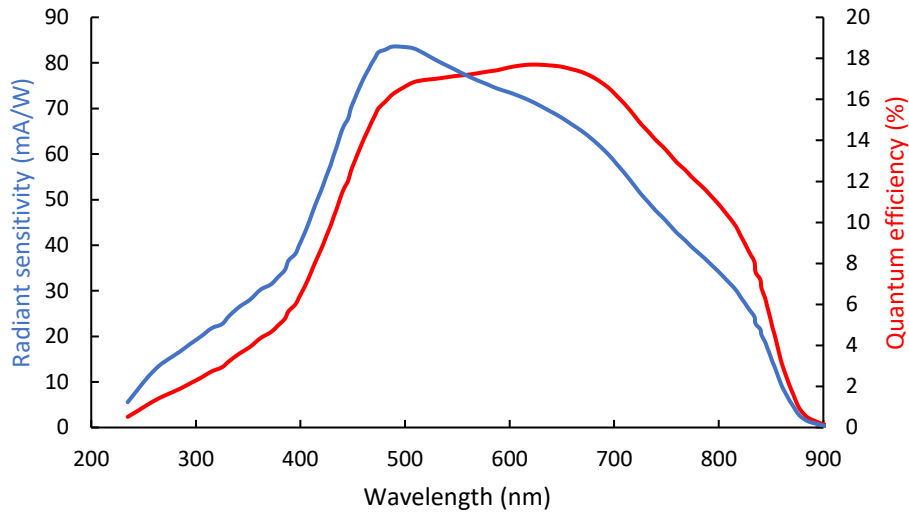


Figure 5 - The radiant sensitivity and quantum efficiency of PM modules as a function of wavelength.

The 3 photomultipliers (Thorlabs PMT1002) operate in a wavelength range from 250 nm to 900 nm. This operating range is dictated by the quantum efficiency of the PM modules, which is zero below 250 nm and above 900 nm. Figure 5 shows the evolution of the quantum efficiency of PM modules as a function of wavelength. A USB-1808X acquisition card (Measurement Computing) is used to digitize the signal. A schematic diagram of the pyrometer is shown in Figure 6, where the three pyrometers are labeled PM1, PM2 and PM3.

For this study, three wavelengths have been used ( $\lambda_1 = 630 \text{ nm}$ ,  $\lambda_2 = 720 \text{ nm}$  and  $\lambda_3 = 820 \text{ nm}$ ). This choice of wavelength is described in detail in Chapter 3. In the following, we assume that the emissivity of condensed species does not vary in this wavelength range.

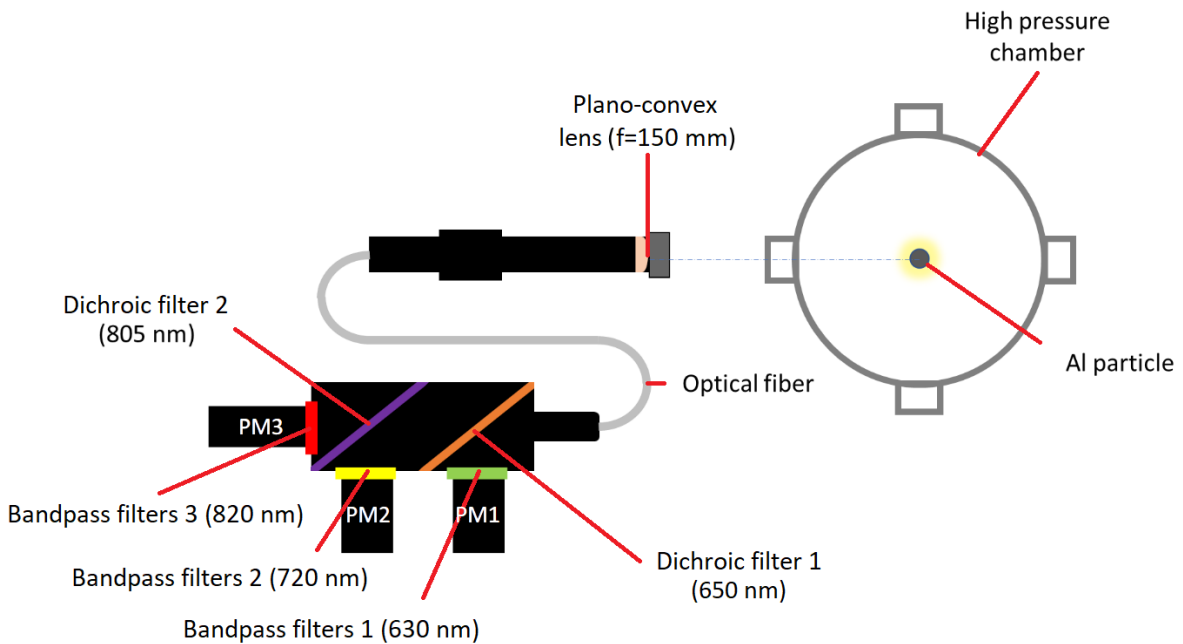


Figure 6 - Schematic of the pyrometer (top view). Plano-convex lens: Thorlabs AC254-150-A. Dichroic filter 1: Thorlabs DMLP650. Dichroic filter 2: Thorlabs DMLP805. Bandpass filters 1: Thorlabs FB630-10. Bandpass filters 2: Thorlabs FB720-10. Bandpass filters 3: Thorlabs FB820-10.

By evaluating the ratio of the radiant intensity measured at the two selected wavelengths,  $\Gamma = L_{\lambda_1}/L_{\lambda_2}$ , we obtain the expression for the temperature based on Planck's law and the Wien approximation:

$$T(\Gamma, \lambda_1, \lambda_2) = \left[ \frac{k}{h \cdot c} \cdot \frac{\lambda_1 \cdot \lambda_2}{\lambda_2 - \lambda_1} \cdot \left( \ln(\Gamma) - 5 \cdot \ln\left(\frac{\lambda_1}{\lambda_2}\right) \right) \right]^{-1}$$

with  $k$  the Boltzmann constant,  $h$  the Planck constant and  $c$  the speed of light.

### 3. Choice of wavelengths and calibration

The choice of spectral splitters, known as dichroic blades, has been optimized to obtain the best compromise between detection and wise separation of the three spectral ranges of the trichromatic pyrometer. The pyrometer's spectral ranges are as follows:

- PM 1 : [580 — 650] nm,
- PM 2 : [650 — 805] nm,
- PM 3 : [805 — 900] nm.

The wavelengths chosen are 630 nm for PM 1, 720 nm for PM 2 and 820 nm for PM 3. To capture only these wavelengths, the PM are fitted with interference filters. These wavelengths have been chosen to avoid emissions from the various gaseous species produced in the reaction zone. These species are detailed in the work of (Dabos et al., 2019). To measure temperature, this article recommends wavelengths beyond the near infrared, which is not possible in our case as the PMs efficiency is zero beyond 900 nm. The emissions and chemiluminescence of species that can be found in afterburning products are listed in Figure 7. The logical choice is between 650 nm and 800 nm to avoid all of the species concerned. According to (Rosenwaks et al., 1975), the chemiluminescence intensity of  $\text{AlO}^*$  could be very low with  $\text{O}_2$  as the oxidizing agent. So, the chemiluminescence and the emission of water vapor should not be impactful under the current conditions studied.

Wavelength (nm)	Shape	Origin
500 at 640	Continuum	Chemiluminescence of $\text{AlO}^*$
300 at 650	Continuum	Chemiluminescence of $\text{CO}_2^*$
309.2 – 394.4 – 396.1	Peak	Emission of Al
464 - 486 - 507	Peak	Emission of AlO
429	Peak	Emission of AlO
500	Peak	Emission of AlO
800 à 1000	Extended peak	Emission of $\text{H}_2\text{O}$
1080 à 1200	Extended peak	

Figure 7 - Emissions and chemiluminescence of species found in afterburning products

Once the wavelengths have been selected, each photomultiplier is calibrated. The pyrometer is calibrated using a reference blackbody (maximum temperature of 3000 K). This method takes into account the optical transmission of the entire optical path and the nonlinear response of the photomultipliers. For this last point, a confidence interval is determined where the temperature measurement is possible if the output voltage of the 2 photomultipliers is greater than 0.2 V and less than 1.5 V. Beyond this interval the response of the photomultipliers is non-linear. The output voltage of each PM is measured for a given blackbody temperature.

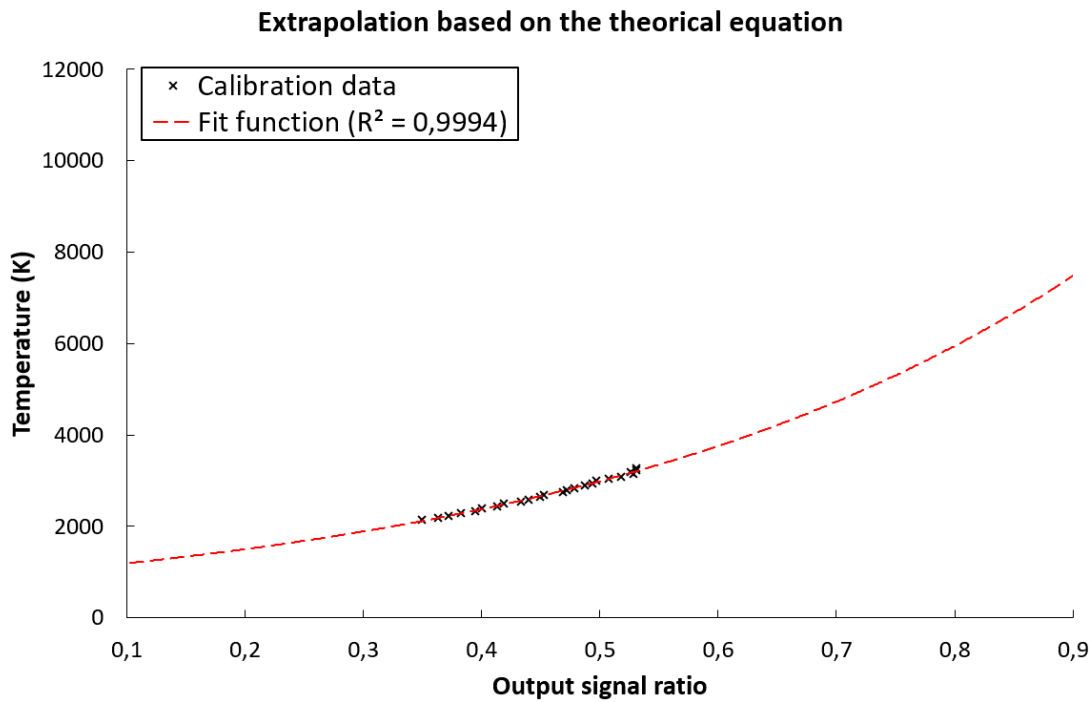


Figure 8 - Temperature of the black body as a function of the ratio between two PMs

Each voltage corresponds to a temperature as illustrated in Figure 8. PMs generate an output voltage that is proportional to the spectral radiance energy multiplied by a calibration factor ( $f_{cal}$ ).

$$\frac{S_1}{S_2} = f_{cal} \times \Gamma$$

with  $S_1$  and  $S_2$  the output voltages generated by the PM and  $f_{cal}$  the proportionality factor obtained by the calibration of the PM (1.2 from our calibration). The temperature calculation is then possible using:

$$T(S_1, S_2, \lambda_1, \lambda_2, f_{cal}) = \left[ \frac{k}{h \cdot c} \cdot \frac{\lambda_1 \cdot \lambda_2}{\lambda_2 - \lambda_1} \cdot \left( \ln \left( \frac{S_1/S_2}{f_{cal}} \right) - 5 \cdot \ln \left( \frac{\lambda_1}{\lambda_2} \right) \right) \right]^{-1}$$

Theoretical extrapolation is carried out on the basis of the equations seen in Chapter 2 to measure temperatures beyond the calibration limits (above 3000 K). Given the very high  $R^2$ , the agreement between the experimental data and the theoretical calculation of these data is excellent, so we admit that the uncertainty is less than 1% in the temperature measurement.

In this study, the pyrometric system only operates with 2 PM (PM1 and PM3), as the output signal from the second photomultiplier never enters the confidence interval for temperature measurement. In future studies, the system will be adapted to remedy this and to operate with 3 PM.

#### 4. Description of the combustion process

Aluminum particles with a diameter of around 70  $\mu\text{m}$  were selected for this study. They are ignited and burnt in air. Note that the laser is automatically switched off once ignition is detected by the rise of the signal on the photomultipliers.

The combustion process is illustrated in Figure 9. All images are captured at the same intensity scale, it is therefore possible to compare their direct radiation. First, the ignition phase is observed when the solid particle (Figure 9–0) becomes liquid (Figure 9–1). This phase is identified by the change in the shape of the particle, from irregular to spherical. The combustion process begins and the laser is stopped after 2.25 ms, when the combustion intensity exceeds a specific detection threshold. After ignition, aluminum vapor is produced and reacts with the oxidizing environment, creating a lobe corresponding to the particle's brightest point. The initial alumina layer that naturally covers the particle liquefies at high temperature ( $T_{\text{melting}}(\text{Al}_2\text{O}_3) = 2345 \text{ K}$ ) and concentrates into a floating lobe on the surface of the liquid aluminum droplet (Figure 9–2). Then, a diffusion flame develops around the liquid droplet during the early post-ignition phase. The flame first grows with the reacting gaseous flow to reach an equilibrium position and rapidly becomes established and totally spherical between 2 ms to 11 ms (Figure 9–3), corresponding to the maximum light emission. Aluminum therefore burns in a stable, almost symmetrical vapor phase regime. The droplet diameter and the flame diameter are progressively reduced and the emission signal decreases in proportion to the reduction of the luminous surface (from 4 ms to 11 ms). After a while, combustion enters an asymmetrical regime (Figure 9–4), represented by spinning (Figure 9–5 and Figure 9–6) and jetting, caused by flow disturbances generated by the growing alumina lobe. At the end of combustion, the lobe completely encapsulates the particle (Figure 9–7).

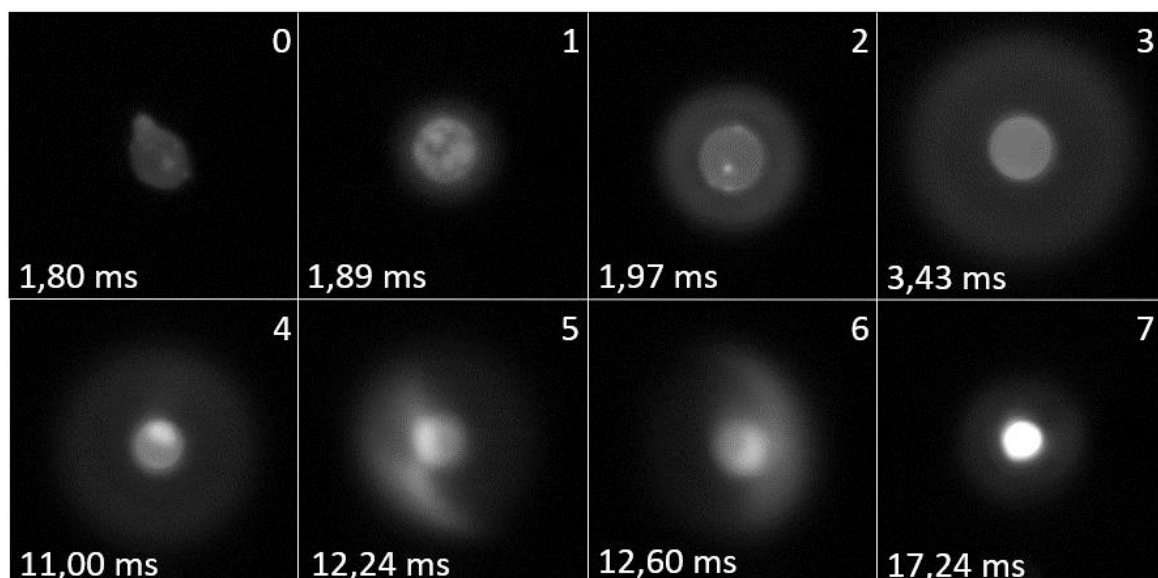


Figure 9 - Images extracted from a combustion sequence of an Al particle in atmospheric air. (initial diameter = 78  $\mu\text{m}$ , sequence captured at 78 000 fps with an exposure time of 12  $\mu\text{s}$  for each images)

## 5. Results

The temporal evolution of the condensed phase temperature after ignition is reported in Figure 10. This plot shows in black, the temperature measured during combustion of an aluminum particle in air. In orange, the evolution of the PM output voltage ( $\lambda_3 = 830$  nm) has been plotted to facilitate identification of the different combustion phases.

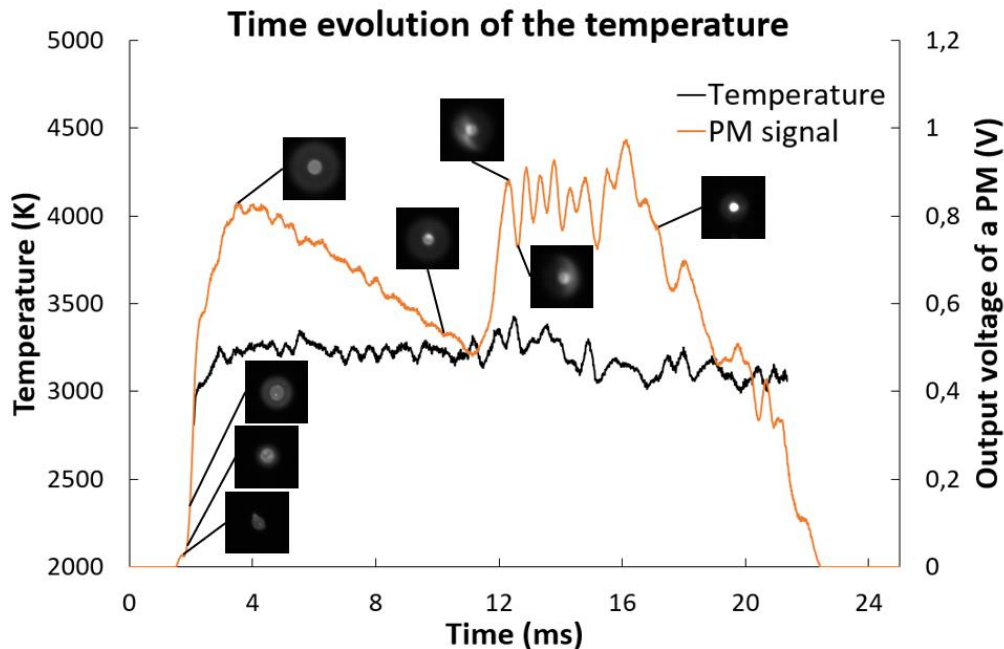


Figure 10 - Time evolution of the temperature of a burning aluminum particle in air at atmospheric pressure (solid black line) and output voltage (solid orange line) of one PM ( $\lambda=830$  nm)

After the ignition phase (about 2.5 ms), an average temperature of about 3250 K is obtained. In Dreizin's various studies, temperatures of around 3000 K (Dreizin, 1996) or around 3500 K (Dreizin, 1999) are measured during the symmetrical combustion phase. Thereafter, the radiation intensity gradually decreases, but the temperature remains constant. This is due to a regression in particle diameter caused by the evaporation of aluminum. The temperature remains stable, however, as combustion is still in progress.

This temperature corresponds to an average between the temperature of the alumina cloud produced in the reaction zone, and the one of the aluminum droplets and its lobe. A similar evolution has been obtained for other particle sizes. This temperature is highly dependent on the phenomena encountered. This method was applied at different pressures, which results are compiled in Figure 10. The raw data presented, are obtained by averaging the temperature obtained during the symmetrical phase. The experiments corresponding to each of the pressure examined are represented on this graph. Each experimental point corresponds to an average temperature obtained during the symmetrical phase. The variability of temperatures observed for an identical pressure depends enormously on the phenomenology observed during the experiment. For example, the size of the initial alumina lobe is a determining factor in the transition from a symmetrical to a spinning-jetting regime.

The temperatures obtained should not be equated with a flame temperature. At present, we are unable to separate the contributions of the aluminum droplet and the oxides produced in the reaction zone.

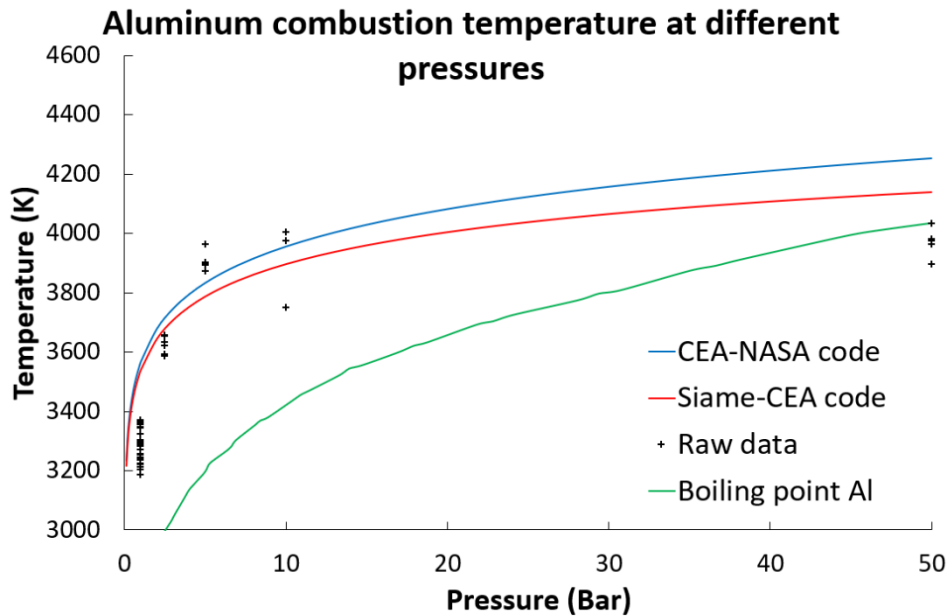


Figure 11 - Aluminum combustion temperature in air at different pressures. Blue curve represents theoretical flame temperature calculations for different pressures using the CEA-NASA calculation code. Red curve illustrates the same calculation, but using the Siame-CEA code. Green curve represents the boiling point of aluminium at different pressure.

However, the temperature obtained can be defined between the aluminum evaporation temperature and the adiabatic flame temperature. The former corresponds to the theoretical temperature of the aluminum droplet, the latter to the maximum combustion temperature. As expected, the measured temperature rises sharply during the first 10 bar and then stabilizes around 4000 K. The adiabatic flame temperatures proposed by the thermochemical codes CEA-NASA (McBride, 2002) and SIAME (Osmont et al., 2018) differ in terms of the intermediate species produced. The variation of aluminum boiling point with pressure is proposed by Sundaram (Sundaram et al., 2015) and increases from 2792 K at atmospheric pressure to around 4000 K at 50 bar. It can be seen that the raw data fall within these temperature limits, except for 50 bar as the symmetrical phase is not correctly defined which may cause this underestimation.

## Conclusion

This study proposes an experimental determination of the temperature involved in the combustion of an aluminum particle. This first approach enabled us to determine the average temperature of the condensed species, composed of a liquid aluminum droplet and oxide nanoparticles produced in the reaction zone. The temperatures obtained are determined during the symmetrical phase of combustion. As pressure increases, this phase shortens and the plateau is rapidly exceeded, followed by a gradual drop in temperature. Most of the raw data lies between the adiabatic flame temperature and the aluminum vaporization temperature (as for the condition at 1 bar where the average temperature is 3300 K for an adiabatic flame temperature measure between 3550 and 3600 K). Measurements taken at 5 bar are highly scattered (approximately 3400 to 4000 K), as the phenomena encountered at this pressure is very variable depending on the behavior of the alumina lobe and its retro-action on the aluminum particle. Temperature measurements are therefore dependent on the phenomenology

observed, it's possible to separate the identical phenomena from each other for the particular condition at 5 bar to reduce the spread of the results.

The maximum laser intensity was used in the experiments described here as the power deposited only affects the ignition delay, without impacting the subsequent combustion sequence. These unique experimental measurements provide both a better understanding of the fundamental combustion of aluminum and a broader database, affording new targets for simulations.

One way of improvement would be to use multichromatic pyrometry with a camera. Preliminary work based on Bucher's studies (Bucher et al., 1998) for calculating the temperature of a 3D element with a 2D image was initiated. This would enable us to target the areas of interest, whatever the phenomenology, in order to propose temperature-related laws as a function of the flame or the aluminum droplet, for example. The measurement made here is an average of the contributions of these two components. The main limitation of our method is the estimation of the size of alumina nanoparticles in the flame. Indeed, this latter parameter is very important in determining the emissivity value of nanometric alumina according to Mie's theory, thus significantly restricting the accuracy of the temperature measurement. It is therefore impossible to separate the different contributions without this information on the size of the alumina particles formed in the cloud. This work is the subject of a specific study aiming to simultaneously estimate the volume fraction of the alumina cloud and the average size of the nanoparticles.

## References

- Bar-Ziv, E. & Sarofim, A. F. 1991. The electrodynamic chamber: A tool for studying high temperature kinetics involving liquid and solid particles. *Prog. Energy Combust. Sci.*, 17 (1):1-65. doi:10.1016/0360-1285(91)90002-5.
- Braconnier, A. 2020. *Etude expérimentale de la combustion d'une particule d'aluminium isolée: influence de la pression et de la composition de l'atmosphère oxydante*. Ph.D. Thesis, Orléans University.
- Bucher, P., Yetter, R. A., Dryer, F. L., Parr, T. P. & Hanson-Parr, D. M. 1998. PLIF species and ratiometric temperature measurements of aluminum particle combustion in O<sub>2</sub>, CO<sub>2</sub> and N<sub>2</sub>O oxidizers, and comparison with model calculations. *Symp. (Int.) Combust.*, 27 (2):2421-2429. doi:10.1016/S0082-0784(98)80094-5.
- Chang, P.-J., Mogi, T. & Dobashi, R. 2021. An investigation on the dust explosion of micron and nano scale aluminium particles. *Journal of Loss Prevention in the Process Industries*, 70:104437. doi:10.1016/j.jlp.2021.104437.
- Cooper, M. A., Kaneshige, M. J., Pahl, R., Snedigar, S. & Renlund, A. 2006. Methods for evaluating aluminized RDX explosives, *Proceeding of the 13th international detonation symposium, Norfolk, Virginia*.
- Dabos, M., Tran, K.-H., Lecysyn, N., Baudin, G., Genetier, M., Ranc, I., Serio, B. & Osmont, A. 2019. Investigation of alumina's emission in the deflagration of gas-aluminum particles mixtures, *Europyro*, Tours, France. Af3P (Association Française des Poudres, Propulsion et Pyrotechnie).
- Davis, E. J., Buehler, M. F. & Ward, T. L. 1990. The double-ring electrodynamic balance for microparticle characterization. *Rev. Sci. Instrum.*, 61 (4):1281-1288. doi:10.1063/1.1141227.
- Dreizin, E. L. 1996. Experimental study of stages in aluminium particle combustion in air. *Combust. Flame*, 105 (4):541-556. doi:10.1016/0010-2180(95)00224-3.

- Dreizin, E. L. 1999. Experimental study of aluminum particle flame evolution in normal and micro-gravity. *Combust. Flame*, 116 (3):323-333. doi:10.1016/S0010-2180(97)00331-3.
- Fedina, K. 2017. *Post-Detonation Afterburning of High Explosives*. Ph.D. Thesis, Lund University.
- Frost, D. & Zhang, F. 2006. The nature of heterogeneous blast explosives, *Proceedings of the 19th International Symposium on Military Aspects of Blast and Shock*, Calgary, Canada. 1-6.
- Hartung, W. H. & Avedisian, C. T. 1992. On the electrodynamic balance. *Proc. R. Soc. Lond. Ser. A: Math. Phys. Sci.*, 437:237-266. doi:10.1098/rspa.1992.0060.
- Legrand, B. 2000. *Etude de la combustion de particules d'aluminium et de magnésium : influence de la composition du mélange gazeux et de la pression*. Ph.D. Thesis, Orléans University.
- Levendis, Y. A., Estrada, K. R. & Hottel, H. C. 1992. Development of multicolor pyrometers to monitor the transient response of burning carbonaceous particles. *Rev. Sci. Instrum.*, 63 (7):3608-3622. doi:10.1063/1.1143586.
- Marion, M. 1996. *Etude sur la Combustion des particules d'aluminium sous pression*. Ph.D. Thesis, Orléans University.
- Mcbride, B. J. 2002. *NASA Glenn coefficients for calculating thermodynamic properties of individual species*, Cleveland, Ohio, USA: National Aeronautics and Space Administration, John H. Glenn Research Center ....
- Millogo, M., Bernard, S. & Gillard, P. 2020. Combustion characteristics of pure aluminum and aluminum alloys powders. *Journal of Loss Prevention in the Process Industries*, 68:104270. doi:10.1016/j.jlp.2020.104270.
- Monier, R., Thumerel, F., Chapuis, J., Soulié, F. & Bordreuil, C. 2017. Liquid metals surface temperature fields measurements with a two-colour pyrometer. *Measurement*, 101:72-80. doi:10.1016/j.measurement.2016.12.031.
- Oran, E. S. 2015. Understanding explosions – From catastrophic accidents to creation of the universe. *Proc. Combust. Inst.*, 35 (1):1-35. doi:10.1016/j.proci.2014.08.019.
- Osmont, A., Genetier, M. & Baudin, G. 2018. Ability of thermochemical calculation to treat organic peroxides. *AIP Conf. Proc.*, 1799 (1):150030. doi:10.1063/1.5044986.
- Panagiotou, T., Levendis, Y. & Delichatsios, M. 1996. Measurements of particle flame temperatures using three-color optical pyrometry. *Combust. Flame*, 104 (3):272-287. doi:10.1016/0010-2180(95)00119-0.
- Rosenwaks, S., Steele, R. E. & Broida, H. P. 1975. Chemiluminescence of AlO. *J. Chem. Phys.*, 63 (5):1963-1965. doi:10.1063/1.431530.
- Suarez, J. 2020. *Modélisation de la combustion diphasique de l'aluminium et application sur la post-combustion d'une charge explosive condensée dans l'air*. Ph.D. Thesis, Toulouse University.
- Sundaram, D. S., Yang, V. & Zarko, V. E. 2015. Combustion of nano aluminum particles (Review). *Combust. Explos. Shock Waves*, 51 (2):173-196. doi:10.1134/s0010508215020045.